Energy-based yield criterion for PMMA from large-scale molecular dynamics simulations

Eugenio Jaramillo, Nathaniel Wilson, Stephen Christensen, Jonathan Gosse, and Alejandro Strachan

Phys. Rev. B **85**, 024114 — Published 17 January 2012

DOI: 10.1103/PhysRevB.85.024114

Energy-based yield criterion for PMMA from large-scale MD simulations

Eugenio Jaramillo,[1] Nathaniel Wilson,[2] Stephen Christensen,[3] Jonathan Gosse,[3] and Alejandro Strachan[2,#]
[1]Department of Chemistry and Biology,
Texas A&M International University, Laredo, TX 78041, USA
[2]School of Materials Engineering and Birck Nanotechnology Center
Purdue University, West Lafayette, Indiana 47907, USA
[3] The Boeing Company,
P.O. Box 3707 MC 42-27, Seattle, WA 98124, USA

We use molecular dynamics (MD) with the DREIDING force field to characterize the ultimate mechanical response of amorphous PMMA. We characterize how volumetric and deviatoric strains contribute to yield for a wide range of loading conditions from pure deviatoric, volume-conserving, cases to isotropic volume expansion. We propose and apply an energy-based yield criterion to define yield consistently for all cases. Our results show that permanent deformation occurs when either the deviatoric or volumetric strains reach critical values except in a narrow region around the transformation between deviatoric- and volumetric-dominated yield where the two strain invariants interact. In contrast, the pressure-modified von Mises criterion is only applicable to shear dominated loading conditions. These results provide insight into the physics of yield in amorphous polymers and provide quantitative information and guidance for physics-based yield criteria for polymer-matrix composite materials.

Keywords: glassy polymer, molecular dynamics, PMMA, thermoplastic, mechanical properties.

I. INTRODUCTION

Understanding the molecular origins of the mechanical response of amorphous polymers remains one of the main challenges in materials science and condensed matter physics. Such an understanding together with quantitative computational models are not only relevant from the point of view of basic science but have the potential to help design new materials with improved properties and impact a wide variety of established industries like aerospace[1] and electronics[2] as well as emerging technologies like micro-electromechanical systems.[3] The mechanical response of crystalline materials is well understood in terms of processes involving the motion of defects including dislocations, grain boundaries and vacancies and such understanding has enabled the development of physics-based, predictive, models for these materials. Much less is known in the case of amorphous polymers. Despite progress in the experimental characterization mechanisms responsible for inelastic deformation and

Corresponding author Email: strachan@purdue.edu

fracture[4] and theoretical advances at the molecular level,[5,6,7,8,9] in thermodynamically consistent viscoelastic modeling[10] and failure criteria[11,12] little is known regarding the conditions associated with the onset of permanent deformation. The use of polymers as matrix in composites pose additional challenges since they experience a wide range of loads including various amounts of deviatoric and dilational loads due to the constraints imposed by the stiffer reinforcements. Experimental studies for complex tri-axial deformation states are challenging and there is limited data for the wide range of conditions experienced by polymeric composite matrices. On the other hand, atomistic simulations have the potential to help fill this gap in understanding as the increase in computing power enables larger-scale simulations and advances in simulation techniques improve the accuracy of the predictions. State-of-the-art molecular dynamics (MD) simulations of polymers can achieve length-scales of tens of nanometers and timescales of tens to hundreds of nanoseconds and while these are small compared to most experiments of interest these simulations can provide a valuable link between atomic processes and macroscopic response, see for example Refs. [5,13,14,15]. Such simulations have provided valuable insight of the mechanisms of post yield softening and hardening and the role of thermal history on mechanical response.[8] Atomistic simulations are also ideally suited to characterize the effect of size[16,17] and molecular structure[6,18] on thermo-mechanical properties. Significant efforts have been devoted to studying the role of tri-axial loading and the molecular mechanisms responsible for yield;[5,19] however work so far has focused on applying the pressure-modified von Mises yield criteria; this assumes deviatoric stresses to be the driving force for inelastic deformation and is not applicable to the wide range of deformations dominated by the dilatational component.

In this paper we use large-scale MD to characterize the onset of permanent deformation for a family of deformations spanning from volume conserving uniaxial to isotropic expansion designed to capture the transition from deviatoric- to volumetric-dominated irreversible deformation. We propose an energy-based yield definition applicable to any deformation path and characterize the yield conditions for the entire family of deformations. Our results indicate that a strain invariant yield criterion can describe the entire family of deformations except for a narrow region around the transition between deviatoric-dominated and volumetric-dominated yield.

The paper is organized as follows. Section II describes the simulation details including deformation paths and analysis; Section III describes the stress-strain behavior obtained for the various simulations. Section IV describes the analysis of our results in terms of the commonly used pressure-modified von Mises yield criterion and Section V presents a more generally applicable energy-based yield criterion and the results of this analysis. Finally conclusions are drawn in Section VI.

II. SIMULATION DETAILS

A. Atomic model preparation

We use the DREIDING force field[20] to describe atomic interactions with partial atomic charges for electrostatic interactions from the Gasteiger method.[21] A cutoff of 12 Å is used for all non-bond interactions during thermalization runs while the PPPM method[22] is used to describe electrostatics during the deformation simulations. All MD simulations are performed using the LAMMPS code from Sandia National Laboratories[23]. All systems consist of PMMA chains with 96 monomers each; 80% of

the chains are syndiotactic and 20% atactic. The simulation cells contain 1080 chains for a total 1,557,360 atoms; this leads to a relaxed (300 K and 1 atm) cubic simulation cells with length 24.173 nm. The initial structures for our simulations are built at low density (0.95 g/cm^3) and high temperature (500 K) using the commercial software MAPS.[24] These structures are then compressed to atmospheric pressure using isothermal MD simulations and then cooled down to T=300 K using isothermal and isobaric MD simulation with a rate of 1.25 K/ps. The effect of cooling rate and size is currently being studied in detail[25] but our preliminary results indicate that, while the mechanical response of the polymer is affected by cooling rate and (to a less degree) size, the main results of this paper, i.e. the relative role of volumetric and deviatoric deformation on yield and the strain invariant yield criterion, remain valid when the cooling rate is reduced by a factor of 10 to 0.125 K/ps. Physical aging denotes the non-chemical relaxation that amorphous polymers undergo with time at temperatures below their glass transition. Both simulations, see for example Refs. [18,26], and experiments[27] have shown that aging leads to an increase in yield stress (with little change in the corresponding yield strain). This aging process can be reversed by deformation (rejuvenation) as can be observed by the flow stress of polymers with different thermal histories collapsing into a common curve after yield.

B. MD simulations of mechanical deformation

Starting with the structures described above, we use non-equilibrium MD to characterize their mechanical response under a variety of loading conditions. The simulation cell is deformed in small increments at each MD step using the following engineering strain tensor:

$$\begin{vmatrix} \xi_x \Delta\varepsilon_l & 0 & 0 \\ 0 & \xi_y \Delta\varepsilon_l & 0 \\ 0 & 0 & \Delta\varepsilon_l \end{vmatrix} \qquad (1)$$

The incremental engineering strain in the longitudinal direction ($\Delta\varepsilon_l$) is kept constant throughout each simulation and it determines the length of the simulation cell as a function of MD step, i, as $[L(i)-L(i-1)]/L(0)=\Delta\varepsilon_l$. We adjust the response in the transverse directions to achieve varying amounts of deviatoric and volumetric strains. We explored the following deformation pathways: i) volume conserving uniaxial with $\xi_x=\xi_y$ both adjusted to conserve volume (for small deformations $\xi_x=\xi_y=-0.5$), and ii) uniaxial deformations with constant transverse to longitudinal strain ratios with values from $\xi_x=\xi_y=-0.33$ to $\xi_x=\xi_y=1$. Pure uniaxial strain: $\xi_x=\xi_y=0$ and isotropic expansion: $\xi_x=\xi_y=1$ are special cases of these deformation paths. For completeness, we also performed simulations involving volume conserving pure-shear with $\xi_x=0$ and ξ_y adjusted to conserve volume ($\xi_y=-1$ for small strains). Temperature during the simulations is controlled via a Nose-Hoover thermostat with coupling constant of 0.1 ps. The presence of the thermostat does not affect our results, as can be seen in the supplementary material[28] where stress-strain curves are compared with results obtained from microcanonical MD simulations (NVE ensemble). We studied two strain rates along the z direction $\Delta\varepsilon_l/\Delta t$ (where Δt is the MD time step) 3.75 10^8 1/s and 1.855 10^8 1/s. While these rates are large compared with experiments (except for shock loading) they are typical of MD simulations due to the relatively short timescales accessible and have been shown to be appropriate to provide insight into yield in polymeric systems.

C. Analysis of the MD runs

A widely used approach to study the results of different loading conditions is to separate both stress and strain tensors into their deviatoric and volumetric (or hydrostatic) components. The deviatoric stress is defined as:

$$\sigma_{eff} = \sqrt{1/2\left[\left(\sigma_1 - \sigma_2\right)^2 + \left(\sigma_2 - \sigma_3\right)^2 + \left(\sigma_3 - \sigma_1\right)^2\right]} \tag{2}$$

where σ_i denote stress components along principal axes; we define effective strain in a similar fashion:

$$\varepsilon_{eff} = 3/4\sqrt{1/2\left[\left(\varepsilon_1 - \varepsilon_2\right)^2 + \left(\varepsilon_2 - \varepsilon_3\right)^2 + \left(\varepsilon_3 - \varepsilon_1\right)^2\right]} \tag{3}$$

where strain components are also given in principal axes. Pressure and volumetric strain describe the volume-changing terms:

$$\sigma_{vol} = \frac{\sigma_1 + \sigma_2 + \sigma_3}{3} \tag{4}$$

$$\varepsilon_{vol} = \varepsilon_1 + \varepsilon_2 + \varepsilon_3 . \tag{5}$$

Note that pressure is the negative of the volumetric stress.

III STRESS-STRAIN RELATIONSHIPS FOR VARIOUS LOADING CONDITIONS

Figure 1 shows the temporal evolution of the stress along the principal axes for various loading conditions for a strain rate of 3.75 10^8 1/s. Figure 1(a) corresponds to volume conserving uniaxial deformation where we observe tensile stress along the z direction and compression along x and y. For $\xi_x=\xi_y=0$, i.e. pure uniaxial strain, [Fig. 1(b)] the simulations predict tensile stress in all three directions and a significant decrease in the flow stress after yielding. As the molecular snapshots shown in Fig. 2 demonstrate, the significant drop in flow stress observed for uniaxial strain is associated with cavitation, i.e. the formation of internal voids in the polymer. We note that voids are present in the system and can percolate before they become visible in projections like those shown in Fig. 2.[29] As expected, this process is not observed for volume conserving simulations where we observe very little softening after yield. Uniform expansion, Fig. 1(c), also leads to cavitation and significant post yield softening. Figures 1 and 2 show clear differences in the polymer behavior when deformation is dominated by deviatoric or volumetric strains underscoring the significant challenge involved in developing a generally applicable yield criterion. While there is no ambiguity regarding the nature of the driving force for inelastic deformation for pure deviatoric or pure volumetric deformations, deformation paths involving a combination of deviatoric and volumetric strains, such as the pure uniaxial strain case of Figs. 1(b), 2(c-d), are more difficult to understand.

Figure 3 shows the deviatoric stress vs. deviatoric strain [Fig. 3 (a)] and volumetric stress-volumetric strain [Fig. 3(b)] curves for the various loading conditions corresponding to the slow deformation rates. We see that the two volume-conserving deformations we studied (volume-conserving uniaxial and shear) lead to essentially identical effective stress-strain behavior. The remaining uniaxial tension deformation simulations involve various amounts of volume expansion and Fig. 3(a) shows how the

effective stress and strain decrease as the transverse to longitudinal strain ratio (ξ_x=ξ_y) increases from -0.5 to 1. The fact that the deviatoric stress decreases with increasing volume expansion in the deformation path is the basis for the pressure-modified von Mises criterion for this class of materials.[5,8,30,19]

IV PRESSURE MODIFIED von MISES YIELD CRITERIA

The pressure modified von Mises criterion, that states that irreversible deformation occurs when the deviatoric stress reaches a pressure-dependent critical value, has been used in the past to analyze experiments[30] and simulation results.[5,19] In prior simulations yield stress was defined as a maximum in the effective stress-strain curve or using the offset method. While this fails to acknowledge that irreversible deformation can be driven by volumetric strains, as will be shown in Section V, we apply it to our simulations in order to compare our results with prior experimental and theoretical work.

Figure 4 shows the deviatoric stress as a function of pressure at the yield point for the various loading paths investigated and for the two strain rates used. In agreement with prior molecular simulations[5,19] we observe a linear decrease in deviatoric stress at the yield point with decreasing pressure up to transverse-longitudinal strain ratios of ~0.16. Increasing the strain rate leads to higher yield stresses but similar pressure sensitivity of the linear region of the pressure modified von Mises plot; the slope predictive by our MD simulations is in good agreement with experimental data[30] shown as triangles in Figure 4. The yield stresses obtained from the MD simulations are significantly higher than those in experiments. This is a common result in MD simulations due to the small size of the systems that preclude strain localization and is also due to the large strain rates.

V ENERGY-BASED YIELD POINT AND CRITICAL STRAIN INVARIANTS

The pressure-modified von Mises criterion assumes that the driving force for irreversible deformation is deviatoric, relegating the role of volumetric deformation to a mere modification of the critical deviatoric stress. The data shown so far suggests a more complex picture where volumetric loads can also drive the onset of plastic deformation. In this Section we propose a definition of yield that treats deviatoric and volumetric components on an equal footing and analyze the conditions and stress and strain that lead to yield.

In order to define the yield point in a consistent manner for all possible deformation paths we use the rate of mechanical work performed on the system per unit initial volume:

$$\dot{W}(t) = \frac{1}{V(0)} \sum_{i=1}^{3} V(t)\sigma_{ii}(t) \left. \frac{d\varepsilon_{ii}^{t}}{dt} \right|_{t}$$

where σ_{ij} and ε_{ij}^{t} are the stress and true strain tensors along the principal axes. This is computed from the simulation using stress and cell lengths (L_i) at discrete times, $n\Delta t$:

$$\dot{W}(n\Delta t) = \frac{1}{V(0)} \sum_{i=1}^{3} V(n)\sigma_{ii}(n) \frac{L_i(n+1) - L_i(n-1)}{2L(n)\Delta t}$$

Figure 5 shows the temporal evolution of the mechanical work per unit time for the slow deformation rate and the various deformation paths. In all cases $\dot{W}$ increases with time early in the deformation process; as the stress required to continue the deformation at constant rate increases so does the mechanical work per unit time performed on the system. We define the onset of irreversible deformation, or yield point, as the condition of maximum mechanical work per unit time for constant strain rate deformation. With this definition, yield marks the point beyond which less work per unit time is required to continue deforming the polymer at a constant rate. Consequently, under load-controlled conditions the material becomes unstable. The proposed definition is consistent with standard definitions for simple loading conditions (e.g. maximum stress in uniaxial tension experiments, where the transverse stress remains zero, and maximum pressure for isotropic expansion) but can be equally applied to any deformation path as opposed to prior definitions used in simulations. An important feature of our approach is that it does not make any assumption regarding whether deviatoric or volumetric strains dominate deformation. In fact, as will be described below, our simulations and analysis enable us to quantify the relative amounts of effective and volumetric strain that lead to yielding as a function of loading path. Additionally we monitor the total mechanical work performed on the polymer up to the yield stress by integrating $\dot{W}(t)$ in time up to the yield point:

$$\Delta W^{Y} = \int_{o}^{t_{yield}} \dot{W}(t)dt$$

Finally, since the rate of deformation has a strong influence on mechanical response a measure that can be applied to all deformation paths would be highly desirable. We cannot use strain rate because it is a tensorial quantity and no effective strain can be applied to the entire family of deformation paths. Thus, consistent with our definition of yield, we use the initial slope of the $\dot{W}$ vs. time curves, that is, the rate of change of the mechanical work per unit volume. This quantity will be denoted effective deformation rate.

Figure 6 shows the deviatoric, Fig. 6(a), and volumetric, Fig. 6(b), strains at the yield point, ε_{dev}^{Y} and ε_{vol}^{Y} respectively, as a function of effective deformation rate; these points are obtained from the two deformation rates studied for each path (only one actual point is shown for $\xi_x=\xi_y=1$ and $\xi_x=\xi_y=0.5$ due to the scale of the plot but two simulations are analyzed in each case). Figures 6(c) and 6(d) show the deviatoric and volumetric stress at yield also as a function of deformation rate and Fig. 7 shows the rate dependence of ΔW^{Y}, the total mechanical work input into the system up to yield. These plots show the important, and path dependent, role of deformation rate in yielding and the importance to compare results at equivalent rates. To do this we extrapolate the MD results (yield strains, stresses and mechanical work) to zero deformation rate assuming linear relationships. These extrapolations are done to evaluate yield for the various paths at comparable deformation rates and are not expected to represent true low strain-rate results due to the linear relationship assumed.

Figure 8 (a) shows the deviatoric and volumetric strains at the yield point as a function the transverse to longitudinal strain ratio for all the simulations performed. Figure 8(b) show the deviatoric and volumetric stresses corresponding to yield as a function of ξ. As expected, the amount of deviatoric strain and stress at onset decrease as the volumetric components increase with increasing ξ. Figure 8 makes it very clear that the

driving force for a large number of the deformation paths explored is volumetric and explains why the pressure modified von Mises criterion only apply to low ξ cases. An analysis of the yield strains shows that, except for a narrow set of conditions near ξ=-0.1, yield occurs when either the deviatoric or volumetric strain reach a critical value (around 11% in our simulations). Even for the conditions near the transition between deviatoric-dominated to volumetric-dominated deformations the critical strains are only about 20% smaller than the asymptotic critical values. In contrast, the stress values at yield show larger variability. This is consistent with the observation that yield stress is more sensitive to processing and deformation conditions than yield strain, see for example Ref. [18]. These results are consistent with the strain invariant failure theory (SIFT) obtained empirically from experimental testing of composites.[11,31]

Finally, Figure 8(c) shows the total work done on the polymer up to yield as a function of transverse to longitudinal strain ratio. Our simulations show a relatively constant energy for volumetric-dominated deformations and a continuous decrease as the relative amount of shear increases. We find volumetric failure to require about 50% more energy than shear-driven yielding.

It is important to stress that our nanoscale samples are essentially defect-free and relatively uniform down to the nanometer scales. The presence of defects in real samples (including micro-cracks, inclusions and voids) is certain to affect the critical strains and energy absorbed up to yield. Furthermore defects are likely to have different effects on the critical volumetric and deviatoric values; we expect micro-cracks and voids to influence the critical volumetric strain more than the deviatoric one. The periodic boundary conditions imposed on the samples limit the maximum wavelength of fluctuations allowed and, consequently, the amount and characteristic size of strain localization that is allowed; this also affects yield and post yield behavior.

We note that the volume conserving shear deformation is not included in Figure 8 since it cannot be described simply by the transverse to longitudinal strain ratio. While the deviatoric stress-strain curve is very similar to that of volume-conserving uniaxial deformation we find the deviatoric strain at yield and energy absorbed to be larger than that of the ξ=–0.5 simulation; this is in part due to the uncertainty in the determination of the yield point in volume conserving paths due to the minimal post-yield softening.

VI. CONCLUSIONS

In summary, we performed large-scale MD simulations to characterize the ultimate mechanical properties of amorphous PMMA for a wide range of loading conditions spanning from purely deviatoric loads to isotropic volume expansion. Such a wide range of loads, while difficult to explore experimentally, is critical to understand and, eventually, improve the polymer performance in composite materials where stiffer reinforcements provide constraints to mechanical load that cause complex tri-axial loading conditions.

An energy-based yield definition enables us to identify the onset of irreversible deformation unambiguously and consistently for the entire family of loading paths. This analysis shows that yield occurs when either the volumetric or deviatoric strains reach a critical value except for a narrow region of loads where the two invariants seem to interact. This yield criterion is applicable over a much wider range of conditions than

the pressure modified von Mises criterion that assumes the driving force for plastic deformation to be deviatoric. Additional work, both experimental and theoretical, to further explore the physics of loading paths where deviatoric and volumetric deformations appear to interact in our simulations is likely to yield interesting new physics and insight into the yield processes of amorphous materials.

The formation of voids such as those observed in pure uniaxial strain is likely to be related to the initial process of crazing that plays a central role in the failure of amorphous polymers.[32] A detailed analysis of the formation and growth of these voids and the structure of the polymer fibrils that develop during deformation could provide insight into the growth of crazes. The transition to a shear-dominated regime as ξ_x and ξ_y is reduced may also provide insight into the transition from crazing to shear dominated regimes.

It is important to stress that the simulations presented here contain no adjustable parameters and that the only fundamental approximations are associated with the interactions between atoms (the force field used) and the use of classical equations of motion. These approximations are unlikely to play a large role on yield envelope for various loading conditions. The high strain rates and relatively small periodic size of the simulations represent practical approximations that also contribute to the differences between MD predictions and experiments; a deeper understanding of their influence on yield requires additional work. Despite these challenges, atomistic and mesoscale simulations are likely to continue providing insight and increasingly quantitative information regarding the ultimate mechanical response of amorphous polymers.

ACKNOWLEDGEMENTS

Work at Purdue was supported by the US National Science Foundation, CMMI Grant 0826356 and by Purdue University. AS, NW and EJ gratefully acknowledge computational resources from nanoHUB.org and support from the Boeing Co.

FIGURE CAPTIONS

FIG. 1. Stress along principal axis as a function of time for three different loading paths: (a) volume-conserving uniaxial, (b) pure uniaxial strain, and (c) volumetric expansion.

FIG. 2. Snapshots of the MD simulations at two different times for volume-conserving uniaxial deformation (a,b) and pure uniaxial strain (c,d).

FIG. 3. Deviatoric (a) and volumetric (b) stress-strain curves for the entire family of deformation paths. Curves are identified by the transverse to longitudinal strain ratios.

FIG. 4. Pressure modified von Mises plot (deviatoric stress at yield vs. pressure) including our MD simulations (squares and circles) and experiments (triangles).

FIG. 5. Mechanical work performed on the samples per unit volume and time for the family of the deformation paths explored. The maximum of these curves define the yield condition.

FIG. 6. Deviatoric and volumetric strains at yield (a,b) and deviatoric and volumetric stresses at yield (c,d) as a function of effective deformation rate for the various deformations. Curves are identified by the transverse to longitudinal strain ratios.

FIG. 7. Total mechanical work absorbed up to yield as a function of effective deformation rate for the various deformations. Curves are identified by the transverse to longitudinal strain ratios.

FIG. 8. Deviatoric and volumetric yield strain (a), yield stress (b) and energy absorbed (c) as a function of transverse/longitudinal strain ratio.

REFERENCES

[1] C. E. Harris, J. H. Starnes, M. J. Shuart, Journal of aircraft, **39** 545-560 (2002).

[2] International technology roadmap for semiconductors 2009 edition, Assembly and Packaging, http://www.itrs.net/Links/2009ITRS/

[3] Behnam Ashrafi, Pascal Hubert, Srikar Vengallatore, Nanotechnology, **17,** 4895-4903 (2006).

[4] M. A. Meyers, V. F. Nesterenko , J. C. LaSalvia, Q. Xue, Materials Science and Engineering **A317** 204 (2001).

[5] D. MacNeill, J. Rottler, Phys. Rev. E 81, 9 (2010).

[6] C. Li and A. Strachan, Polymer 51 6058-6070 (2010).

[7] A. V. Lyulin, M Michels, Phys. Rev. Lett. **99** 085504 (2007).

[8] B. Vorselaars, A. V Lyulin, M. A. J Michels, J. Chem. Phys. **130** 074905 (2009).

[9] M. Warren and J. Rottler, Phys. Rev. Lett. 104, 205501 (2010).

[10] J. M. Caruthers, D. B. Adolf, R. S. Chambers, P. Shrikhande, Polymer, **45** 4577 (2004); D. B. Adolf, R. S. Chambers J. M. Caruthers, Polymer, **45**, 4599 (2004).

[11] J. H. Gosse, S. Christensen, AIAA-2001-1184 (2001).

[12] T. Tay, S, Tan, V, Tan, J. Gosse, Composites Science and Technology, 65, 935 (2005).

[13] A. V. Lyulin, B. Vorselaars, M. A. Mazo, N. K. Balabaev, M. A. J. Michels, Europhys. Lett. **71,** 618-624 (2005).

[14] RA Riggleman, GN Toepperwein, GJ Papakonstantopoulos, JJ de Pablo, Macromolecules, **42**, 3632-3640 (2009).

[15] Robert A Riggleman, Hau-Nan Lee, M. D Ediger, Juan J De Pablo, Soft Matter, **6**, 287 (2010).

[16] J. A. Torres, P. F. Nealey, J. J. de Pablo, Phys. Rev. Lett. **85**, 3221-3224 (2000).

[17] Kenji Yoshimoto, Tushar S Jain, Paul F Nealey, Juan J De Pablo, J. Chem. Phys. **122**, 144712 (2005).

[18] C. Li and A. Strachan, Polymer, **52**, 2920-2928 (2011).

[19] J. Rottler, M. O. Robbins, Phys. Rev. E, **64** , 8 (2001).

[20] S. L. Mayo, B. D. Olafson, W.A. Goddard, III, Journal of Physical Chemistry, **94,** 8897 (1990)

[21] J. Gasteiger, M. Manili, Tetrahedron, **36**, 3219 (1980).

[22] R. W. Hockney and J. W. Eastwood, *Computer Simulation Using Particles*, Adam Hilger, NY (1989).

[23] S. J. Plimpton, J. Comput. Phys. **117**, 1 (1995).

[24] MAPS (The Materials And Processes Simulations platform). Scienomics Inc.; 2008.

[25] N. Wilson, E. Jaramillo and A. Strachan, in preparation.

[26] M Utz, P.G Debenedetti, F.H Stillinger, Phys. Rev. Lett. **84** 1471-1474 (2000).

[27] HGH Van Melick, LE Govaert, HEH Meijer, Polymer, **44**, 3579-3591 (2003).

[28] See supplemental material at http://link.aps.org/supplemental/xxx.

[29] Alejandro Strachan, Tahir Çağın, William A Goddard, Phys. Rev. B, 63, 4 (2001).

[30] R Quinson, J Perez, Journal of Materials Science, 32, 1371-1379 (1997)

[31] LJ Hart-Smith, Phil. Mag. **90**, 4263-4331, (2010).

[32] E. J. Kramer and L. L. Berger, Advances in Polymer Science, **91/92**, 1-68 (1990).

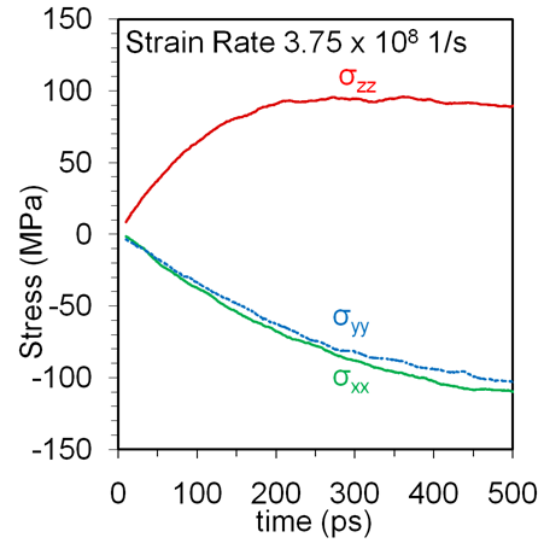
Strain Rate 3.75 x 10^8 1/s
σzz
σyy
σxx
Stress (MPa)
time (ps)
150
100
50
0
-50
-100
-150
0
100
200
300
400
500

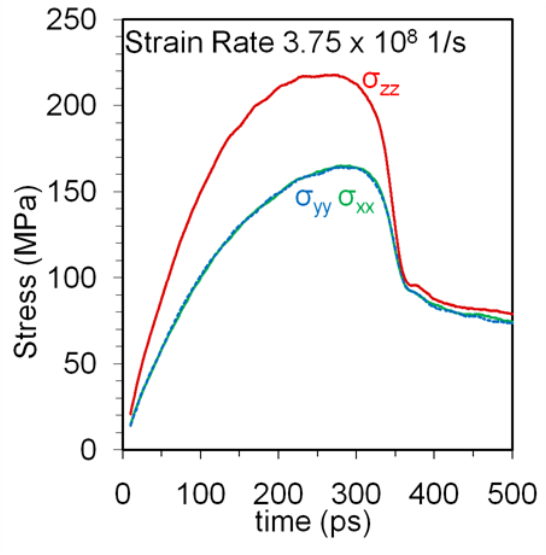
Strain Rate 3.75 x 10^8 1/s
σzz
σyy σxx
Stress (MPa)
time (ps)
250
200
150
100
50
0
0
100
200
300
400
500

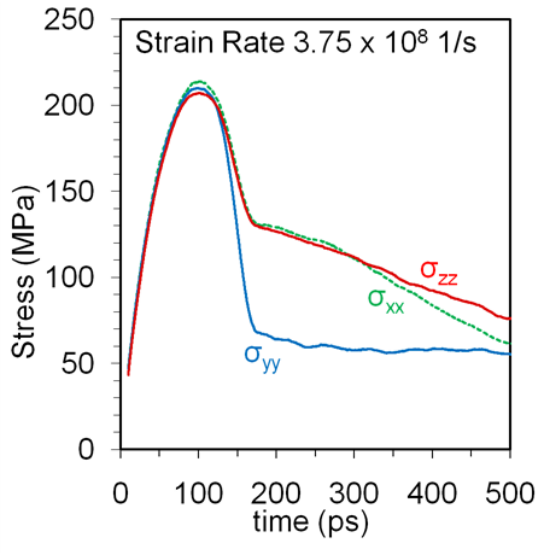
Strain Rate 3.75 x 10^8 1/s
σzz
σxx
σyy
Stress (MPa)
time (ps)
250
200
150
100
50
0
0
100
200
300
400
500

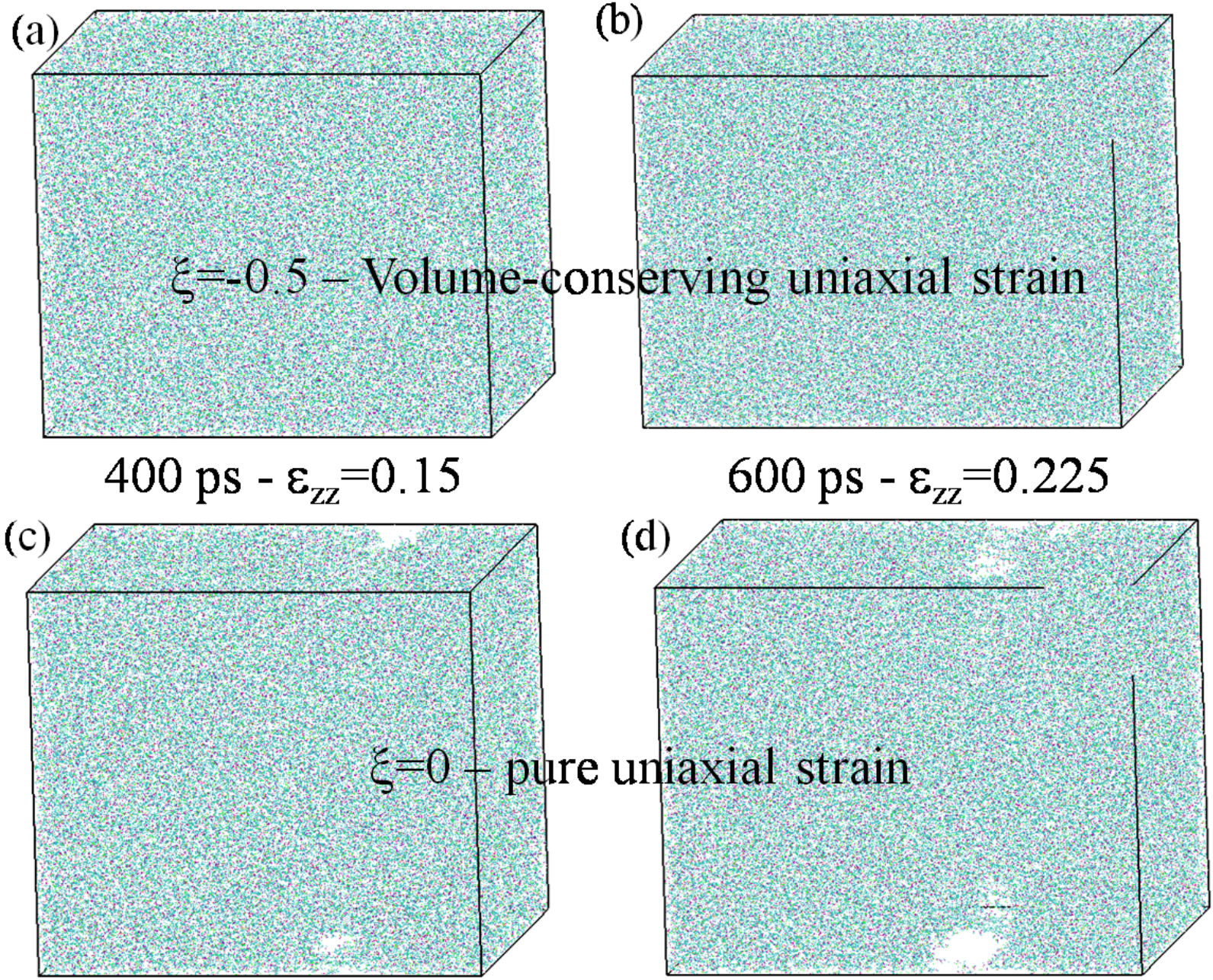
(a)
(b)
ξ=-0.5 – Volume-conserving uniaxial strain
400 ps - εzz=0.15
600 ps - εzz=0.225
(c)
(d)
ξ=0 – pure uniaxial strain

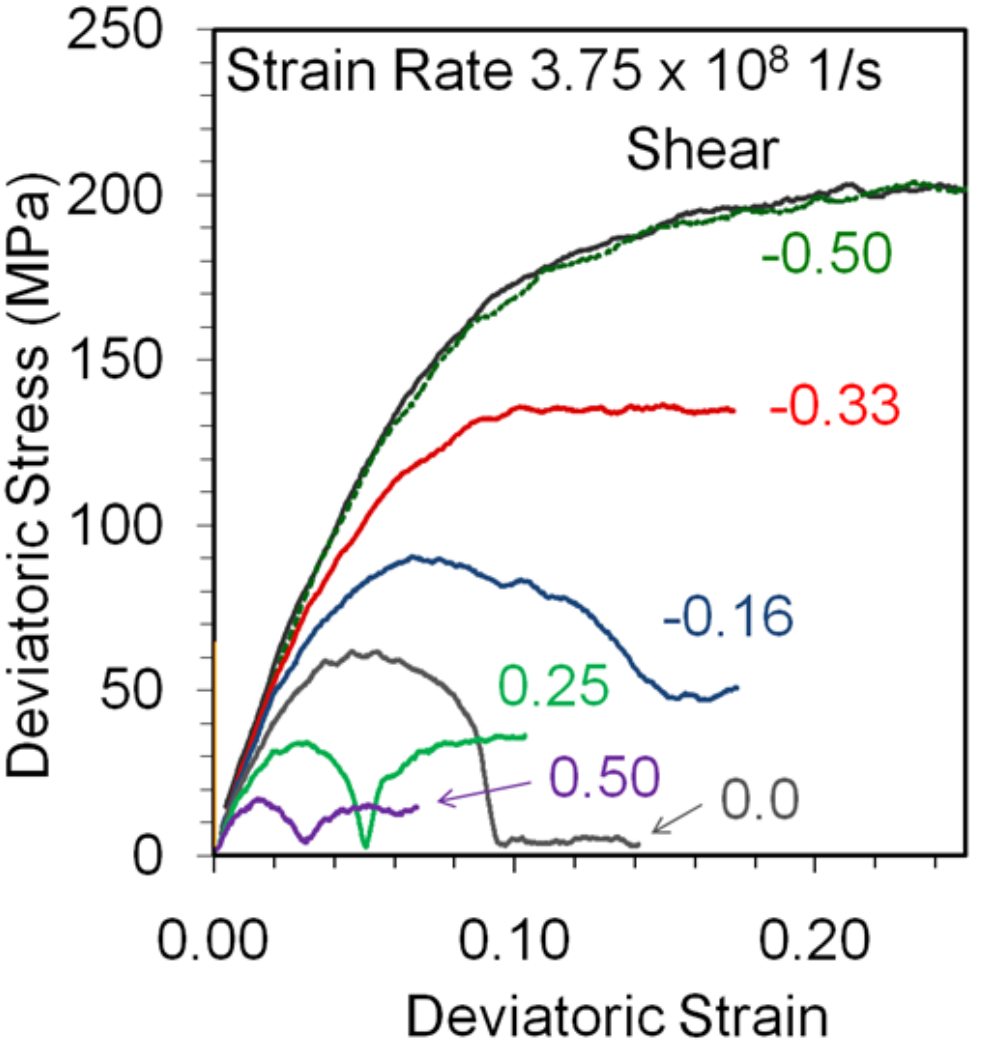
Strain Rate 3.75 x 10^8 1/s
Shear
-0.50
-0.33
-0.16
0.25
0.50
0.0
Deviatoric Stress (MPa)
250
200
150
100
50
0
0.00
0.10
0.20
Deviatoric Strain

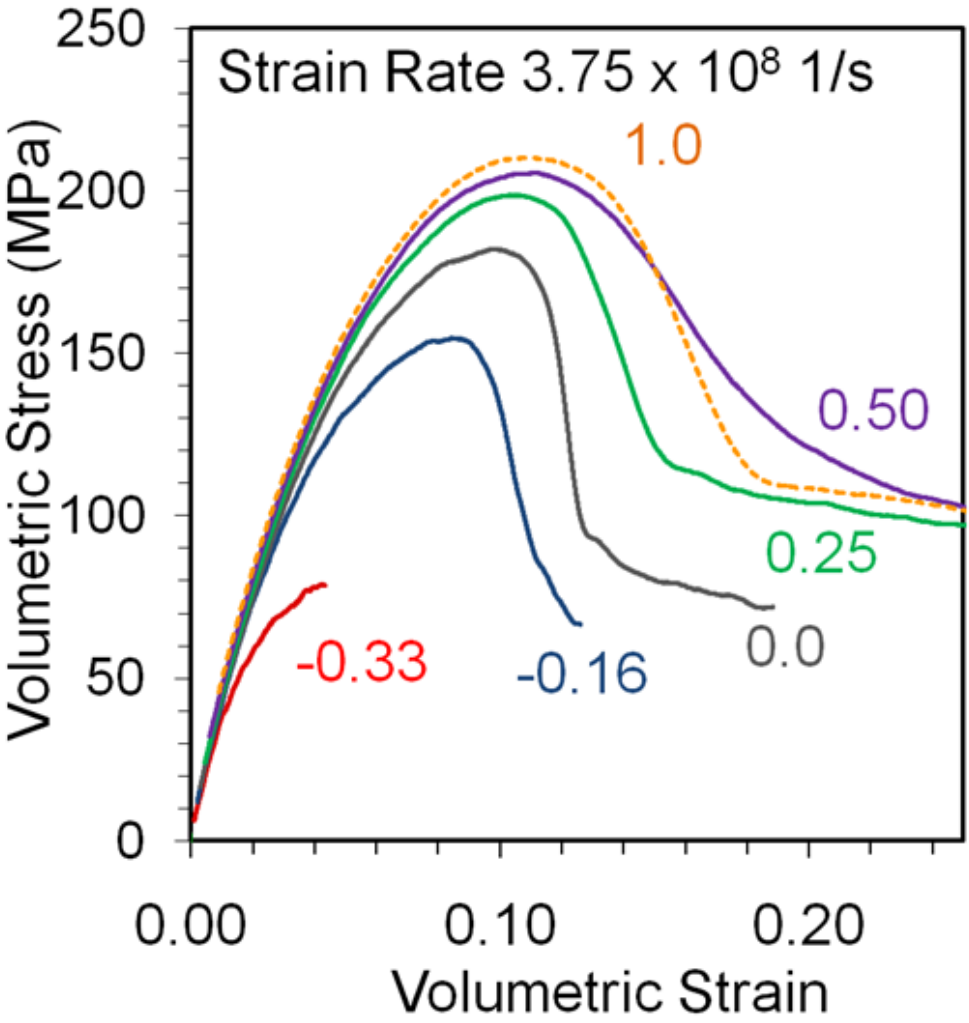
Strain Rate 3.75 x 10^8 1/s
1.0
0.50
0.25
0.0
-0.33
-0.16
Volumetric Stress (MPa)
250
200
150
100
50
0
0.00
0.10
0.20
Volumetric Strain

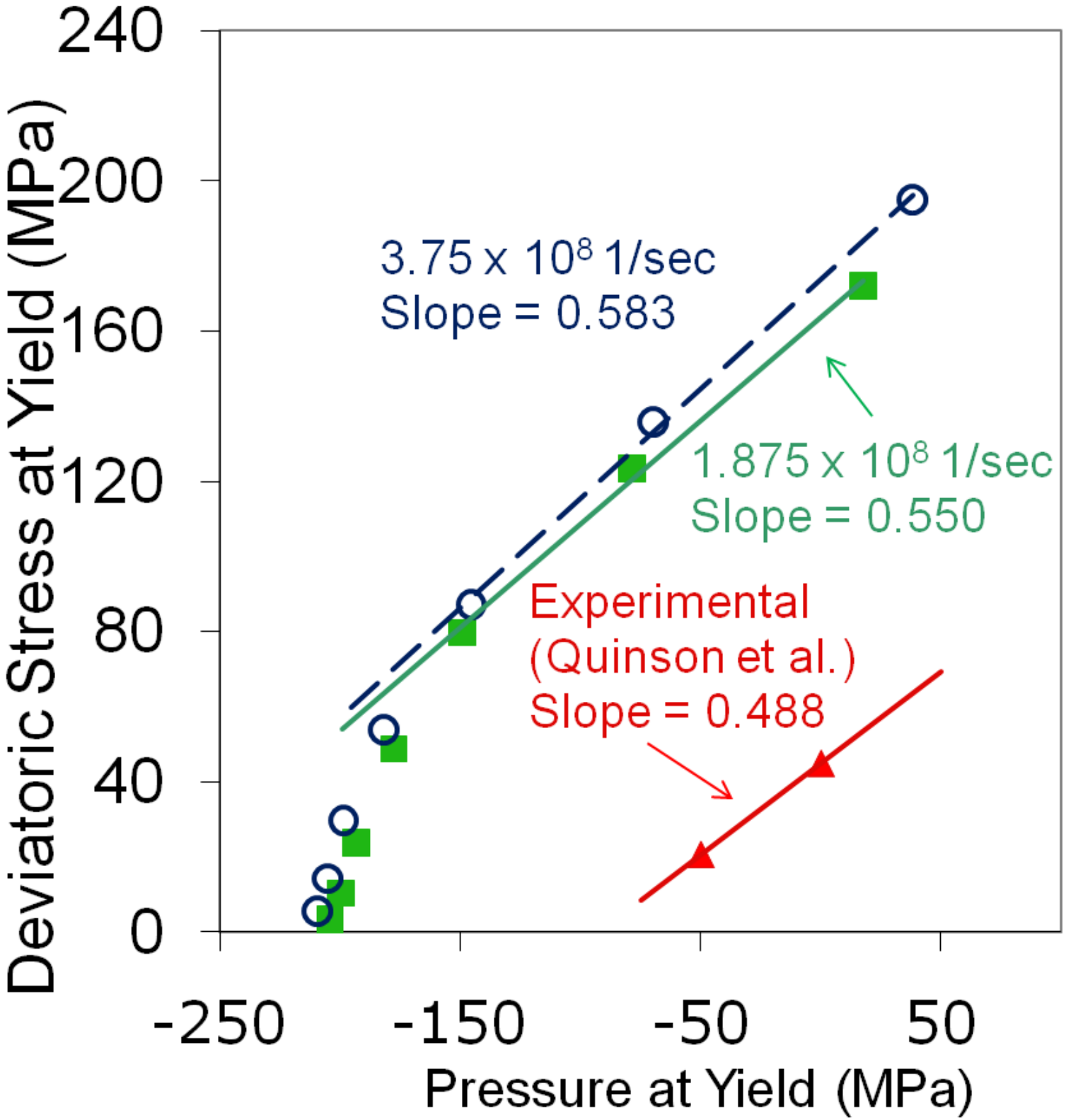
240
200
160
120
80
40
0
Deviatoric Stress at Yield (MPa)
-250
-150
-50
50
Pressure at Yield (MPa)
3.75 x 10^8 1/sec
Slope = 0.583
1.875 x 10^8 1/sec
Slope = 0.550
Experimental
(Quinson et al.)
Slope = 0.488

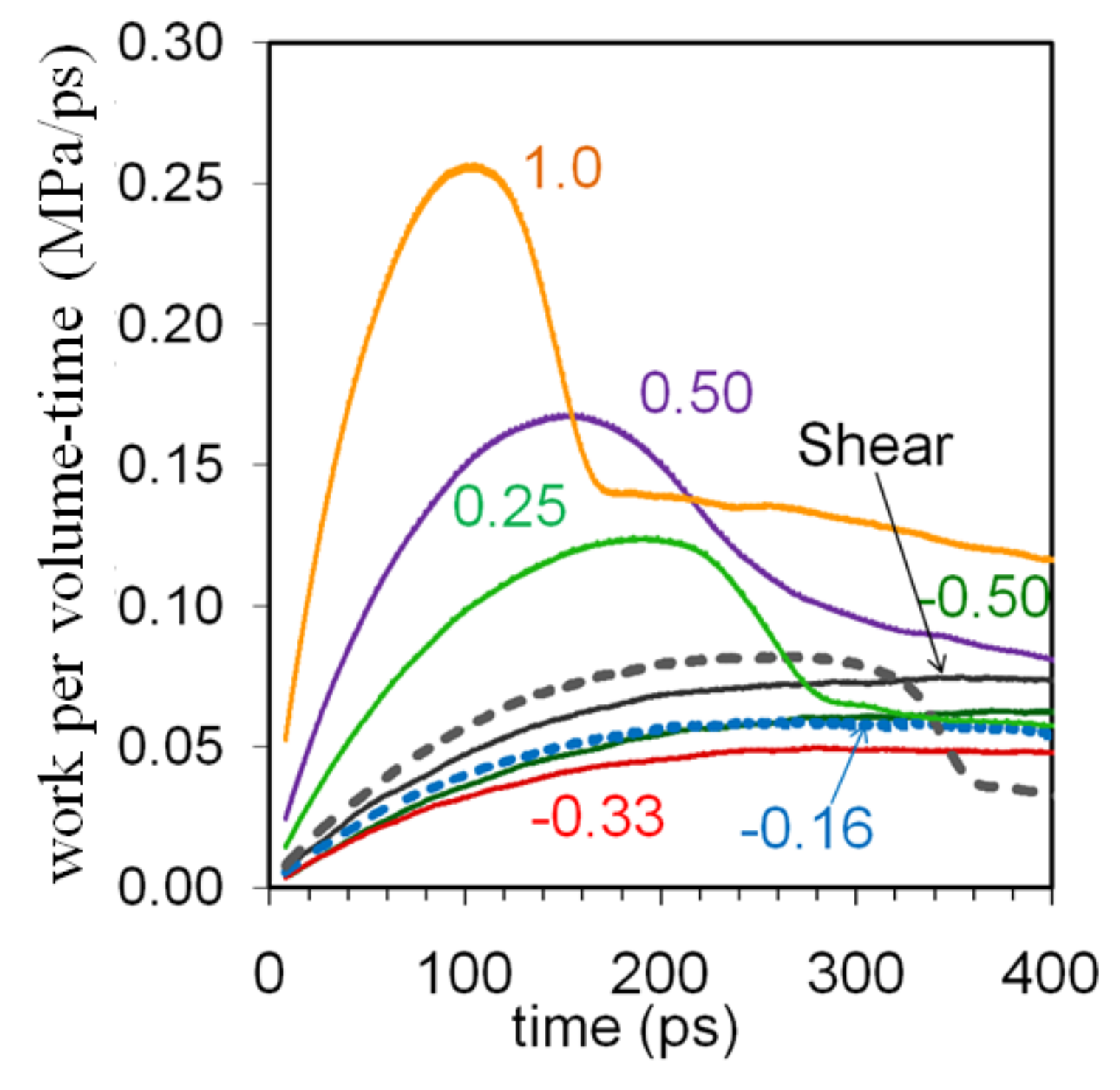
work per volume-time (MPa/ps)
0.30
0.25
0.20
0.15
0.10
0.05
0.00
0
100
200
300
400
time (ps)
1.0
0.50
0.25
Shear
-0.50
-0.33
-0.16

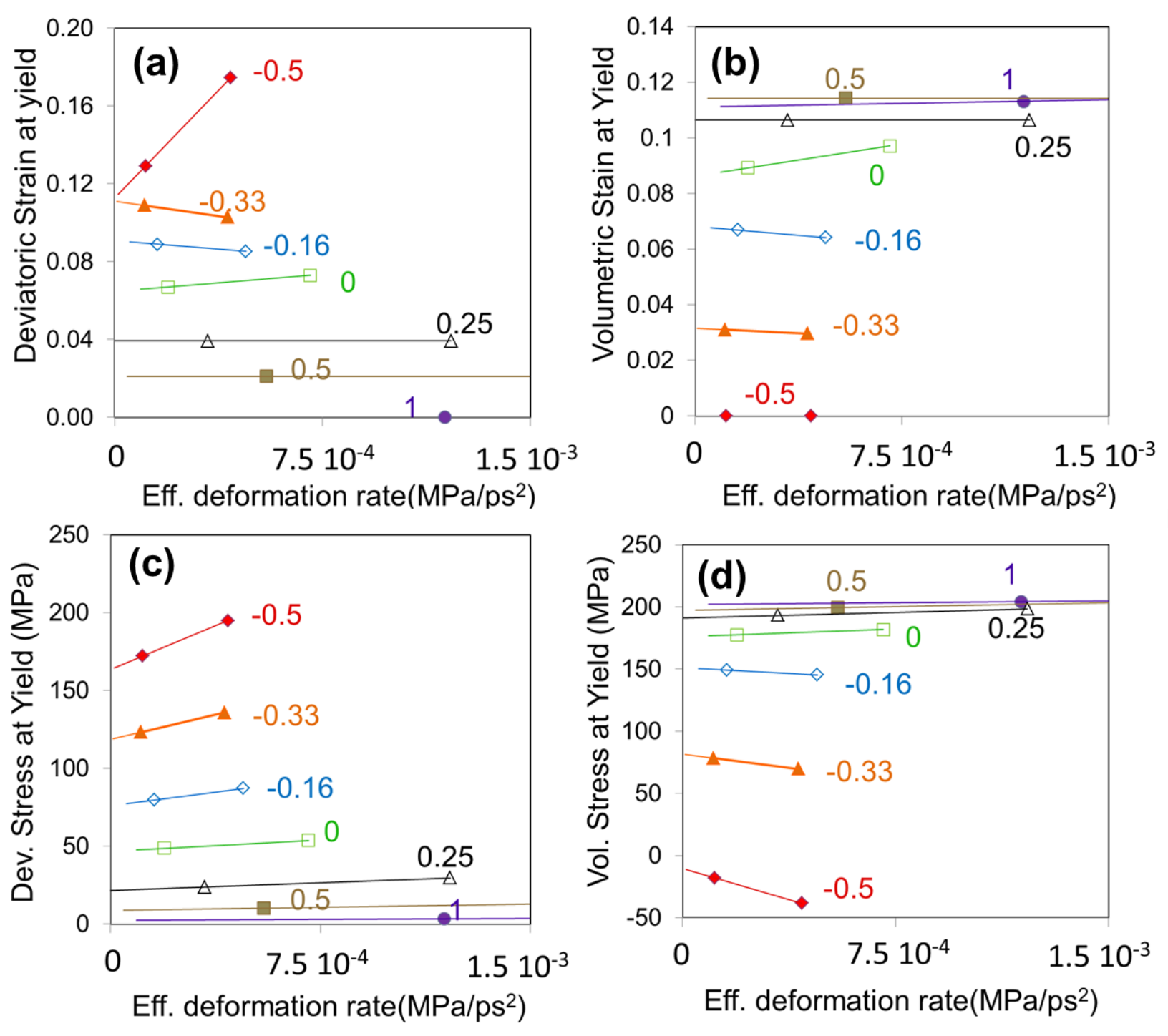
(a)
Deviatoric Strain at yield
0.20
0.16
0.12
0.08
0.04
0.00
-0.5
-0.33
-0.16
0
0.25
0.5
1
0
7.5 10-4
1.5 10-3
Eff. deformation rate(MPa/ps2)
(b)
Volumetric Stain at Yield
0.14
0.12
0.1
0.08
0.06
0.04
0.02
0
0.5
1
0.25
0
-0.16
-0.33
-0.5
0
7.5 10-4
1.5 10-3
Eff. deformation rate(MPa/ps2)
(c)
Dev. Stress at Yield (MPa)
250
200
150
100
50
0
-0.5
-0.33
-0.16
0
0.25
0.5
1
0
7.5 10-4
1.5 10-3
Eff. deformation rate(MPa/ps2)
(d)
Vol. Stress at Yield (MPa)
250
200
150
100
50
0
-50
0.5
1
0.25
0
-0.16
-0.33
-0.5
0
7.5 10-4
1.5 10-3
Eff. deformation rate(MPa/ps2)

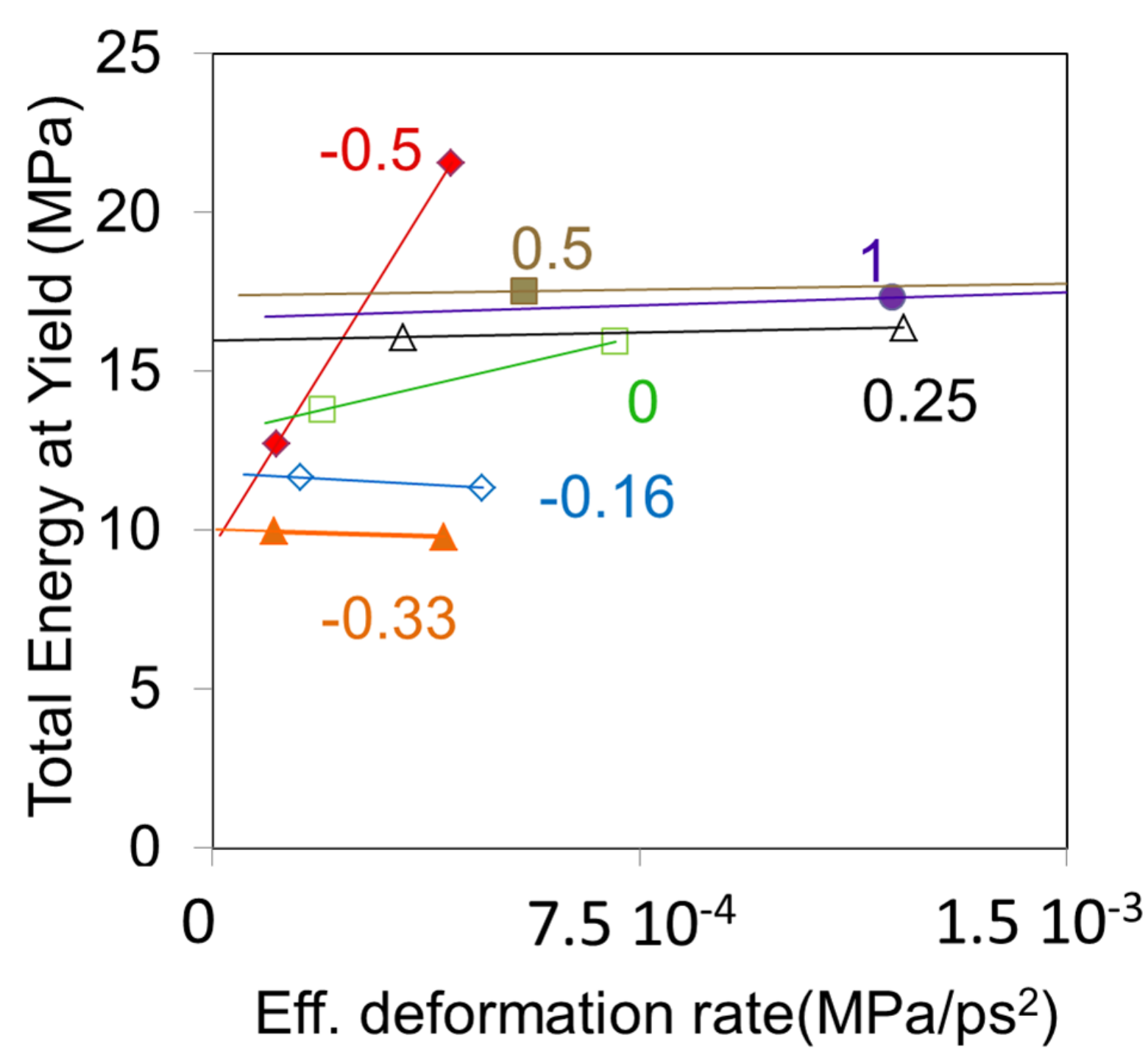
25
20
15
10
5
0
Total Energy at Yield (MPa)
-0.5
0.5
1
0
0.25
-0.16
-0.33
0
7.5 10-4
1.5 10-3
Eff. deformation rate(MPa/ps2)

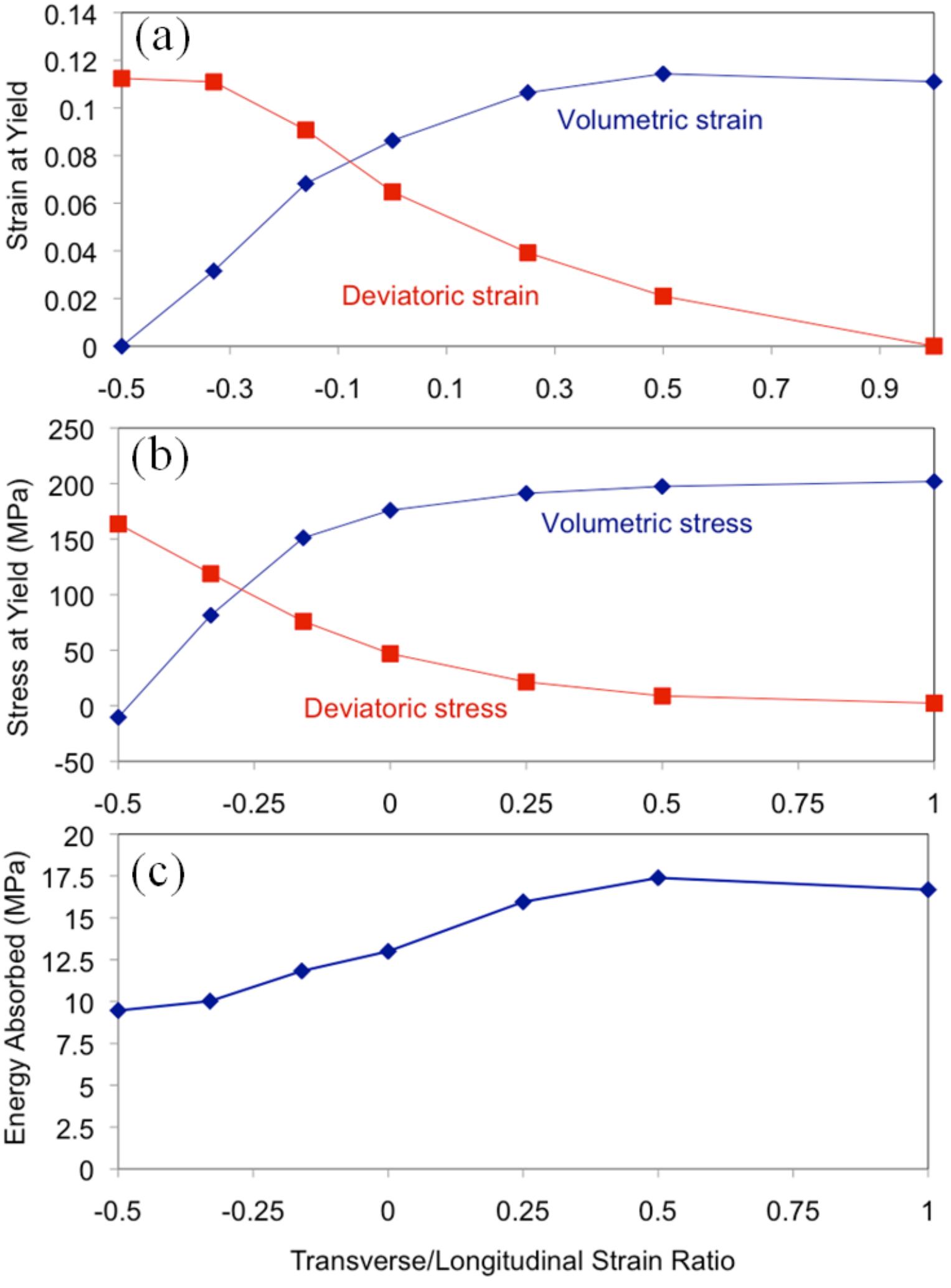
(a)
Strain at Yield
0.14
0.12
0.1
0.08
0.06
0.04
0.02
0
-0.5
-0.3
-0.1
0.1
0.3
0.5
0.7
0.9
Volumetric strain
Deviatoric strain
(b)
Stress at Yield (MPa)
250
200
150
100
50
0
-50
-0.5
-0.25
0
0.25
0.5
0.75
1
Volumetric stress
Deviatoric stress
(c)
Energy Absorbed (MPa)
20
17.5
15
12.5
10
7.5
5
2.5
0
-0.5
-0.25
0
0.25
0.5
0.75
1
Transverse/Longitudinal Strain Ratio